IJAREEIE

e-ISSN: 2278-8875
p-ISSN: 2320-3765

International Journal of Advanced Research in Electrical, Electronics and Instrumentation Engineering

Volume 13, Issue 4, April 2024

INTERNATIONAL STANDARD SERIAL NUMBER INDIA

Impact Factor: 8.317

| e-ISSN: 2278 – 8875, p-ISSN: 2320 – 3765| www.ijareeie.com | Impact Factor: 8.317|| A Monthly Peer Reviewed & Referred Journal |

||Volume 13, Issue 4, April 2024||

|DOI:10.15662/IJAREEIE.2024.1304001 |

A Miniaturized Reconfigurable CPW Square Slot Antenna with Widen Tuning Frequency Region Based on MEMS Technology

Nkembeteh Julius Youchemberng, Leiying Zhai, Nan Jingchang, Hong Zhu

M.Sc. Scholar [CST], Dept. of CST, Liaoning Technical University, China

Professor, [CIE] Dept. of EIE, Liaoning Technical University, China

Professor, [CIE] Dept. of EIE, Liaoning Technical University, China

M.Eng. Scholar [CIE], Dept. of EIE, Liaoning Technical University, China

ABSTRACT: Slot antennas are widely developed for reliable transmission and reception in a wireless communication system. In high-frequency telecommunications applications, slot antennas exhibit low profile design, ease of concealment, and high power transmission with omnidirectional radiation patterns. Some shortcomings still exist in the present research, such as single radiation frequency, narrow bandwidth, low power gain, poor power radiation, large size, and so on. For this reason, a novel reconfigurable CPW-fed slot antenna is proposed in this paper. A tuning quadrilateral ring slot coupled patch antenna with a stub is proposed to make the matching of the resonant frequency tunable. It is realized by adjusting the gap between the stub and the quadrilateral ring slot. Then, the MEMS actuator technology is used to drive the quadrilateral-ring slot path to move for a desired distance. Correspondingly, a desired radiation frequency will be achieved with the bias-driven voltage. The HFSS and ANSYS software are used for the microwave performance and mechanical displacement of the proposed tuning slot antenna. The results show that the displacement is 15.5 µm with a bias voltage of 40 V, and the frequency shifts from 59.79 GHz to 60.4 GHz, with the antenna peak gain of 8.16dBi (bandwidth is 151 MHz). The FEM results show that the 1st frequency is 492.79 Hz which proves the proposed movable system has good resistance to environmental vibration. The researches in this paper prove a kind of design theory for a reconfigurable antenna owing to the virtues of miniaturization, low power consumption, and high reliability.

KEYWORDS: Miniaturization, Reconfigurability, MEMS, Coplanar waveguide, substrate, Quadrilateral-ring slot, Microwave frequency

I. INTRODUCTION

Slot antennas, which are typically used in wireless communications and radar systems, have gained increasing attention due to their compact size, low profile, and potential for frequency adjustability. This has led to the widespread in the design of many passive and active devices at microwave and millimeter-wave [[1] [2] [3] [4]. However, the present problem with solution research of slot antenna in frequency adjustment lies in archiving both broad bandwidths and precise control over the resonant frequency. To resolve those problems, the reconfigurable technology is widely developed in antenna design [5] [6]. Concerning the slot antenna, several methods have been proposed for this problem such as to modify the geometric shape or structure of the slot because of their unique electromagnetic effect in reflection and transmission electromagnetic waves. L. Jin [7] implements doping in parasitic elements to increase frequency tunability. Some researchers [8] [9] utilize frequency-selective surface materials to achieve frequency modulation. With this, slot antennas have enhanced impedance matching, broader bandwidths, and an aptitude to yield simultaneously unidirectional and bidirectional radiation patterns as compared to patch antenna [10][11]. In comparison with the microstrip feed, the slot antenna has low reliance on the characteristic impedance by the substrate thickness and is also easy to integrate with monolithic microwave integrated circuits. The slot antennas with coplanar waveguide feedlines have brought lots of attention in recent years [12] [13]. CPW-fed slot antennas [14] [15] and the impacts of the feed-slot interaction are investigated in the literature [16] [17]. However, the CPW-fed slot antenna is difficult to reconfigure due to an inset structure. Some research is focused on the complicated slot shape or dimension change [18]. However, those frequency reconfigurations rely on PIN diodes or correspond to the different samples. It is not a continuous adjustable method.

| e-ISSN: 2278 – 8875, p-ISSN: 2320 – 3765| www.ijareeie.com | Impact Factor: 8.317|| A Monthly Peer Reviewed & Referred Journal |

||Volume 13, Issue 4, April 2024||

|DOI:10.15662/IJAREEIE.2024.1304001 |

Concerning those problems, a tunable CPW slot antenna adjusted by a MEMS actuator [19] [20] [21] is put forward in this paper. The constant frequency tuning is realized by a constant applied voltage on the MEMS actuator. The slot antenna is built on a silicon device layer with a tuning rectangle-ring structure and a stub. The MEMS actuator is constructed in the device layer corresponding to the tuning ground structure. The gap between the tuning ground structure and the stub can be adjusted by the MEMS actuator. Therefore, the antenna's operating frequency can be modulated dynamically. With a bias voltage of 40 V, the frequency can be altered in a 0.61 GHz frequency width. The proposed antenna has good radiation characteristics in both E and H planes. It proves a good structure for the research of reconfigurable antennae. Section II describes the configuration and design procedures of the antenna. Section III presents the simulation results and discussions. Finally, the paper is concluded in section IV.

II. ANTENNA DESIGN AND PROCEDURES

2.1. Antenna Design Scheme

The 3D model of the reconfigurable antenna is shown in Figure 1. Figure 1(a) shows the 3D model and cross-section along AA'. It is constructed by three parts distributed on three layers. A CPW-fed slot antenna is fabricated on the top layer by the Au sputtering process. A larger view of the CPW-fed slot antenna is displayed in Figure 1(b). A tuning rectangle-ring ground structure is built and a stub is fixed inside it. The slot antenna is fed by the stub feed which is connected from the ground structure to the other end of the entrance of the CPW transmission line. The stub is then coupled to the end of the 50 Ω CPW transmission with a gap 'g' between the signal strip and the coplanar ground structure. The stub is a minimal distance 'S' away from the edge of the ground structure in the center of the rectangle-ring slot. Under the Au layer, it is a silicon device. Between them, the SiO_2 layer is set to form electric isolation. A movable silicon platform is fixed under the tuning rectangle-ring ground structure in the Si device layer. It is anchored by two pairs of fold-beam to the silicon body. Around the movable platform, the movable comb fingers are arranged on it while the fixed comb fingers are arranged on the main Si body. The MEMS actuator is formed by the fixed and movable comb fingers to drive the movable platform. The whole 3D structure in the device layer is fabricated by the DRIE process. The bottom layer is a silicon substrate, which supports the above parts. With a bias voltage on the MEMS actuator, the movable platform can move according to the input electric signal. The detailed symbol meaning and parameter value are represented in Table 1.

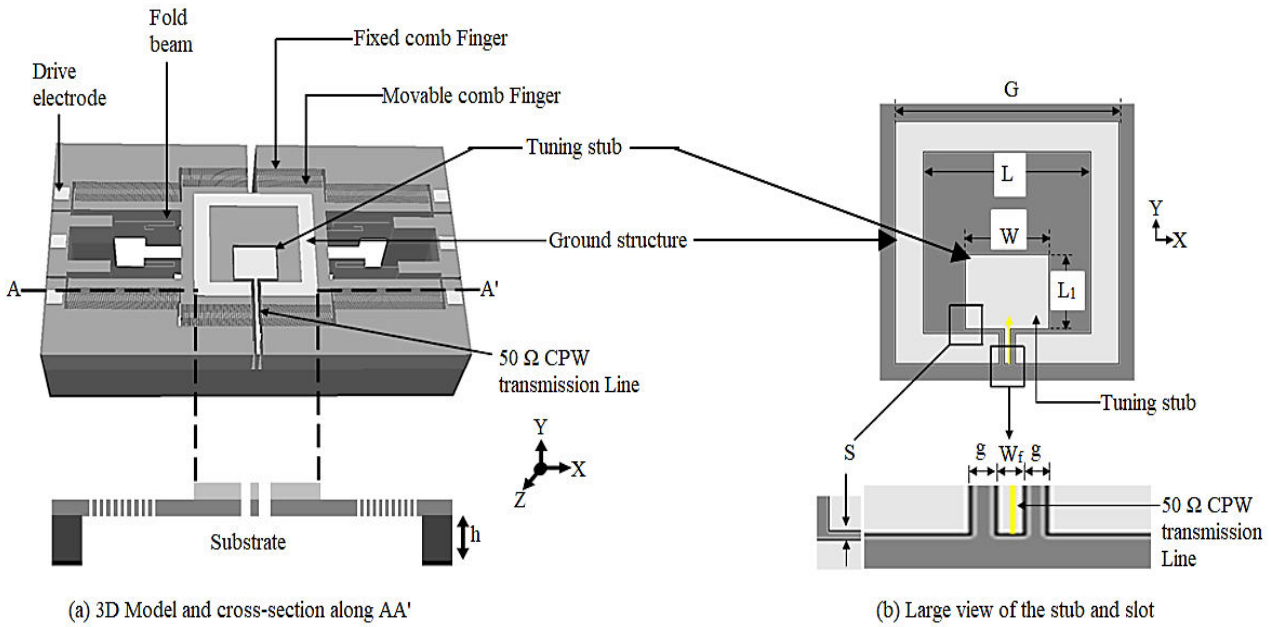

Figure 1: 3D model of reconfigurable antenna

| e-ISSN: 2278 – 8875, p-ISSN: 2320 – 3765| www.ijareeie.com | Impact Factor: 8.317|| A Monthly Peer Reviewed & Referred Journal |

||Volume 13, Issue 4, April 2024||

|DOI:10.15662/IJAREEIE.2024.1304001 |

Table 1: OPTIMIZED PARAMETER

S/N	Symbol	Meaning	Dimensions / µm
1	G	Side Length of the ground plane	2 x 10^3 µm
2	L	Length of the Square radiating slot	1.5 x 10^3 µm
3	W	Width of the tuning stub	750 µm
4	L_1	Length of the tuning stub	610 µm
5	W_f	Width of the fixed metal strip	55 µm
6	g	Distance between the stub feed and the ground structure	45 µm
7	S	Distance between stub and edge of ground structure	40 µm

2.2. MEMS Working Principle

The structure of the MEMS design is demonstrated in Figure 2. It contains comb drive transmissions, fold beams, and other structures. The MEMS actuator is driven by comb-like electrostatic electricity which converts the electrical signal into vertical displacement changes, to realize continuous adjustment of the antenna's frequency. The folding beam is connected between the fixed comb finger and anchor to control mechanical displacement, as compared to a straight cantilever beam. The coefficient of elasticity is reduced, which in turn reduces the driving voltage. The comb transmission is divided into two parts, which are the moving comb finger and the fixed comb finger. By injecting opposite charges into the two groups of combs, and using the attraction between the electrode plates with anisotropic charges, the relative motion of the electrode plates is controlled by controlling the number of charges. It has low power consumption, short response time, easy to complete higher frequency drive, and the structure is also easy to implement. The movable comb fingers are supported by the fold beams and are equity staggered with the fixed comb (the spacing is g_{comb}). The overlapping length of the fixed comb finger and the movable comb finger is X_{comb}. The length of the comb finger and the overlap determine the maximum stroke of the drive. The comb parameters and fold beam values in the device are represented in Table 2 and Table 3 respectively. The formula for calculating this force is expressed in equation 1: (decomposing other functional structures to indicate their specific structure and function).

$$F = \frac{1}{2} \cdot V^2 \cdot \frac{\partial c}{\partial x} = \frac{n_{comb} \cdot \varepsilon \cdot h_{comb} \cdot V^2}{g_{comb}} \quad \text{____ (Equation 1)}$$

Where n_{comb} is the pairwise number of comb teeth, Ɛ is the relative permittivity between plates, and C is the capacitance value of the plate between the overlapping combs fingers, with the fold beams coefficient calculated as expressed in equation 2:

$$K \approx \frac{48GJ}{(L_a)^2 (n_{beam})^3 \left(\frac{GJL_a}{EI_x} + L_b\right)} \quad \text{_____ (Equation 2)}$$

Where G is the torsional modulus, I_X is the moment of inertia, J is the torsional constant, and E is the modulus of elasticity of the shape beam material. When considering the residual stress, the elastic coefficient calculations are extremely complex and so, they are often solved by AnsoftHFSS software. When 0K, after the electrostatic attraction F, and the elastic coefficient k of the folding beam, it can be determined by Hooke's theorem. Hence, the displacement generated by the electrostatic comb drive can be obtained.

| e-ISSN: 2278 – 8875, p-ISSN: 2320 – 3765| www.ijareeie.com | Impact Factor: 8.317|| A Monthly Peer Reviewed & Referred Journal |

||Volume 13, Issue 4, April 2024||

|DOI:10.15662/IJAREEIE.2024.1304001 |

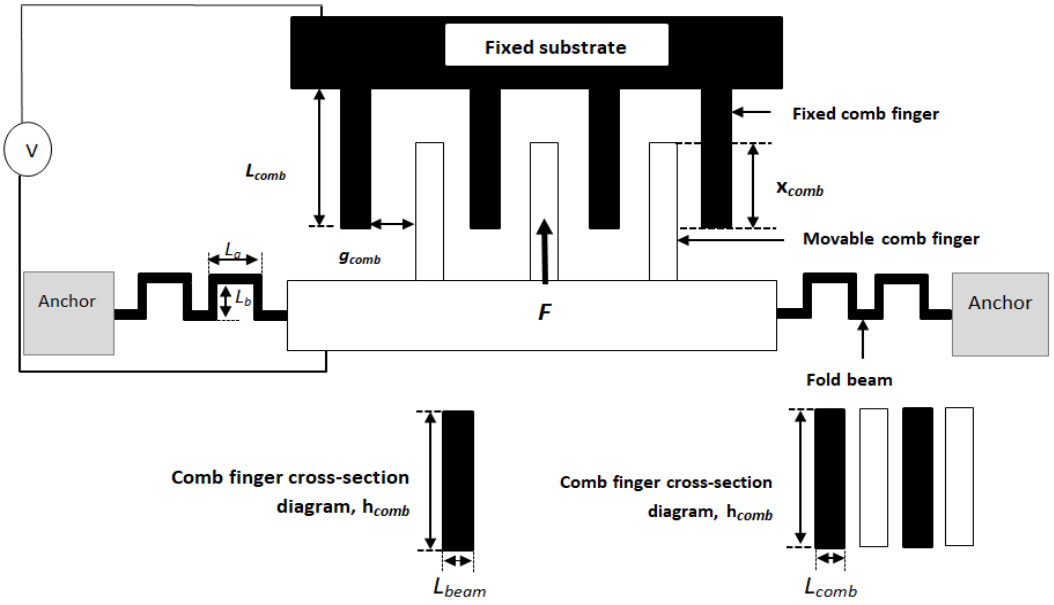

Figure 2: Schematic of the electrostatically driven comb structure

TABLE 2: DRIVING COMB PARAMETER OF MEMS

Parameter	Comb finger Length / µm	Comb finger Width / µm	Comb number	Comb finger Thickness µm	Cantilever Length / µm	Cantilever Width / µm
Value	250 µm	4 µm	220	50 µm	2287 µm	6 µm

TABLE 3: PARAMETERS OF FOLD BEAM

Device layer number	Beam parameter	Value
1	Beam Length (L_{beam1}) / µm	125 µm
	Beam Thickness (h_{beam1}) / µm	3 µm
	Beam Width (t_{beam1}) / µm	40 µm
	Number of beams(n_3)	11
2	Beam Length (L_{beam2}) / µm	120 µm
	Beam Thickness (h_{beam2}) / µm	3.3 µm
	Beam Width (t_{beam2}) / µm	40 µm
	Number of beams(n_4)	11

| e-ISSN: 2278 – 8875, p-ISSN: 2320 – 3765| www.ijareeie.com | Impact Factor: 8.317|| A Monthly Peer Reviewed & Referred Journal |

||Volume 13, Issue 4, April 2024||

|DOI:10.15662/IJAREEIE.2024.1304001 |

III. RESULT AND DISCUSSION

3.1. Static State

The antenna is simulated by HFSS software and the result is successfully obtained and displayed in Figure 3. When the spacing between the tuning stub and quadrilateral ring slot is S = 40 µm, the return loss at S11 < -10 dB records -45dB and -36dB at a frequency range of 59.72 to 59.84 GHz with a bandwidth of 151MHz, and from 60.3 to 60.5 GHz with a bandwidth of 204MHz.

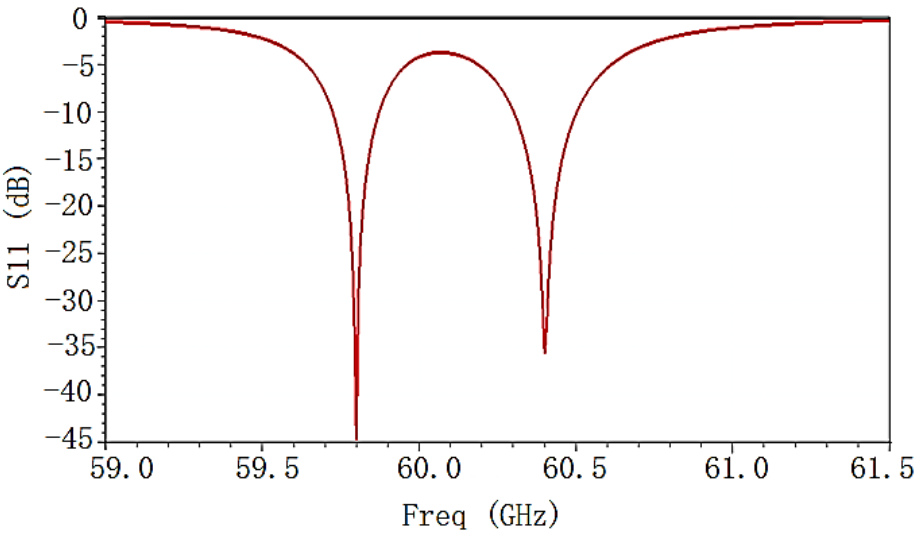

Figure 3: S_{11} results of return loss

3.2. Current distribution and Radiation Pattern of the tunable antenna

The surface current distribution on the tuning stub and the electric field distribution on the square slot of this antenna are determined by HFSS software. It can be seen in Figure 4(a) and (b) that, the current distribution radiates on the top patch side and the feedline on the bottom side of the substrate at 59.8 and 60.4GHz. At 60.4 GHz, the radiation from the vertical component of the electric field is dominant, and the cross-polarization is largely due to the horizontal components of the electric field. Thus, for the present design, these two frequencies are expected to have very few similarities in broadside radiation characteristics along the E-plane (*y*-*z* plane) and H-plane (*x*-*z* plane) as illustrated in Figure 5. From the results, the shift in frequencies has alike polarization planes and radiation patterns. With this, the radiation pattern of the antenna is omnidirectional. The determined maximum and minimum gain of the antenna in the broadside direction is 8.16 and -11.33dBi respectively (Figure 4 c). It can also be seen that both plane patterns show relatively large radiation cross-polarization, which is due to strong horizontal components of the surface current and the electric field. This has led to a significant rise in cross-polarization in radiation.

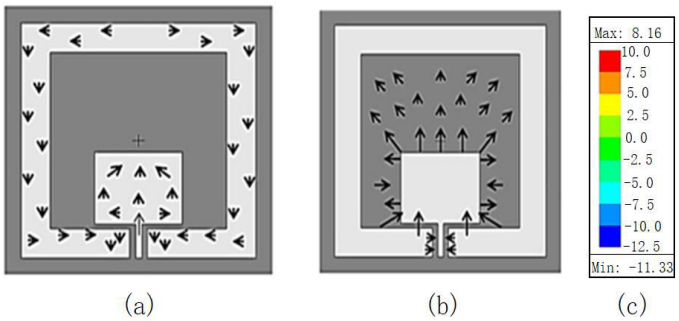

Figure 4: (a) Current distributions on the tuning stub at 59.8 GHz, (b) Electric Field distribution on the square slot at 60.4 GHz, and (c) Maximum and minimum gain of the antenna

| e-ISSN: 2278 – 8875, p-ISSN: 2320 – 3765| www.ijareeie.com | Impact Factor: 8.317|| A Monthly Peer Reviewed & Referred Journal |

||Volume 13, Issue 4, April 2024||

|DOI:10.15662/IJAREEIE.2024.1304001 |

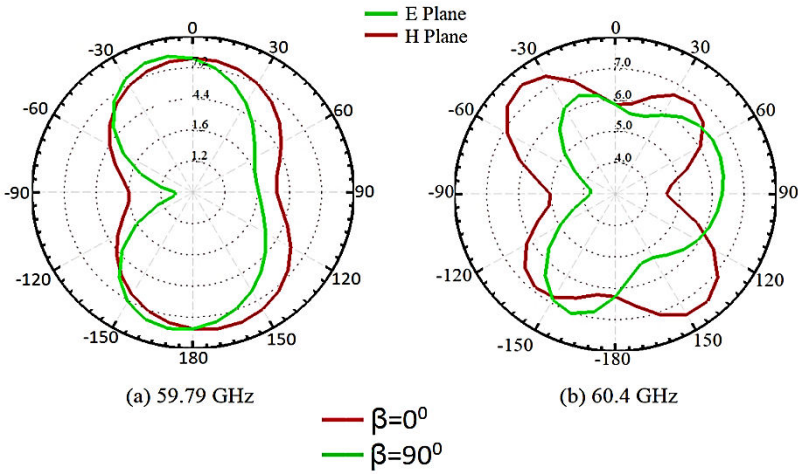

Figure 5: Radiation Pattern of E and H Plane

3.3. Mems comb actuator simulation and discussions

Table 2 shows the parameters of the electrostatic comb driver and structure, a maximum driven voltage of 40 V is loaded between the combs. By using ANSYS software, the elastic system of the fold beam obtained is 1.2 N/m, and the coefficient of elasticity of the bottom beam is 1.8 N/m, such that from Hooke's theorem the displacement of the comb driver and the driving voltage can be obtained. To get the control voltage of the MEMS actuator, AnsoftHFSS software is used for simulation. It can be seen in Figure 6, that the shifts are all 15.5μm with a stress of 40.0 mpa, which implies a depression relationship. When 15.5 μm is attained, the structure of the device layer is obtained. Hence, the moving distance is within the range of the MEMS comb finger, which can meet the requirements of the adjustable antenna frequency for the displacement of the microactuator.

Materials type: Monocrystalline silicon, Breaking stress 600mpa to 7.7gpa [22].

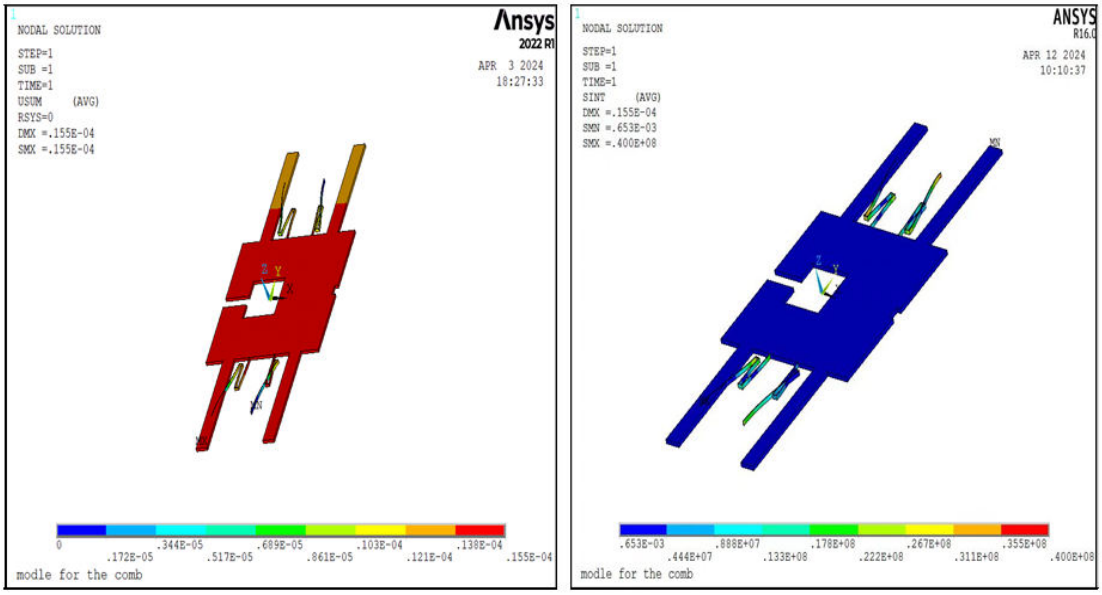

Figure 6: Maximum Displacement and stress cloud maps for movable part

The relationship between the displacement of the MEMS driver and the voltage is seen in Figure 9 a. The displacement of the MEMS actuator from 0.968 to 15.5 μm is accurately controlled by adjusting the voltage in the range of 10 to 40 V, and the control of any resonant frequency is realized as shown in Figure 9 b. To ensure the reliability of MEMS

| e-ISSN: 2278 – 8875, p-ISSN: 2320 – 3765| www.ijareeie.com | Impact Factor: 8.317|| A Monthly Peer Reviewed & Referred Journal |

||Volume 13, Issue 4, April 2024||

|DOI:10.15662/IJAREEIE.2024.1304001 |

actuators, the mechanical properties of the MEMS actuators are simulated. Table 4 shows the frequencies of the first four orders, with their corresponding MEMS modal schematically illustrated in Figure 7.

TABLE 4: FREQUENCIES OF THE FIRST FOUR ORDERS

Mode	First	Second	Third	Fourth
Frequency	492.79	638.01	841.8	1589.9

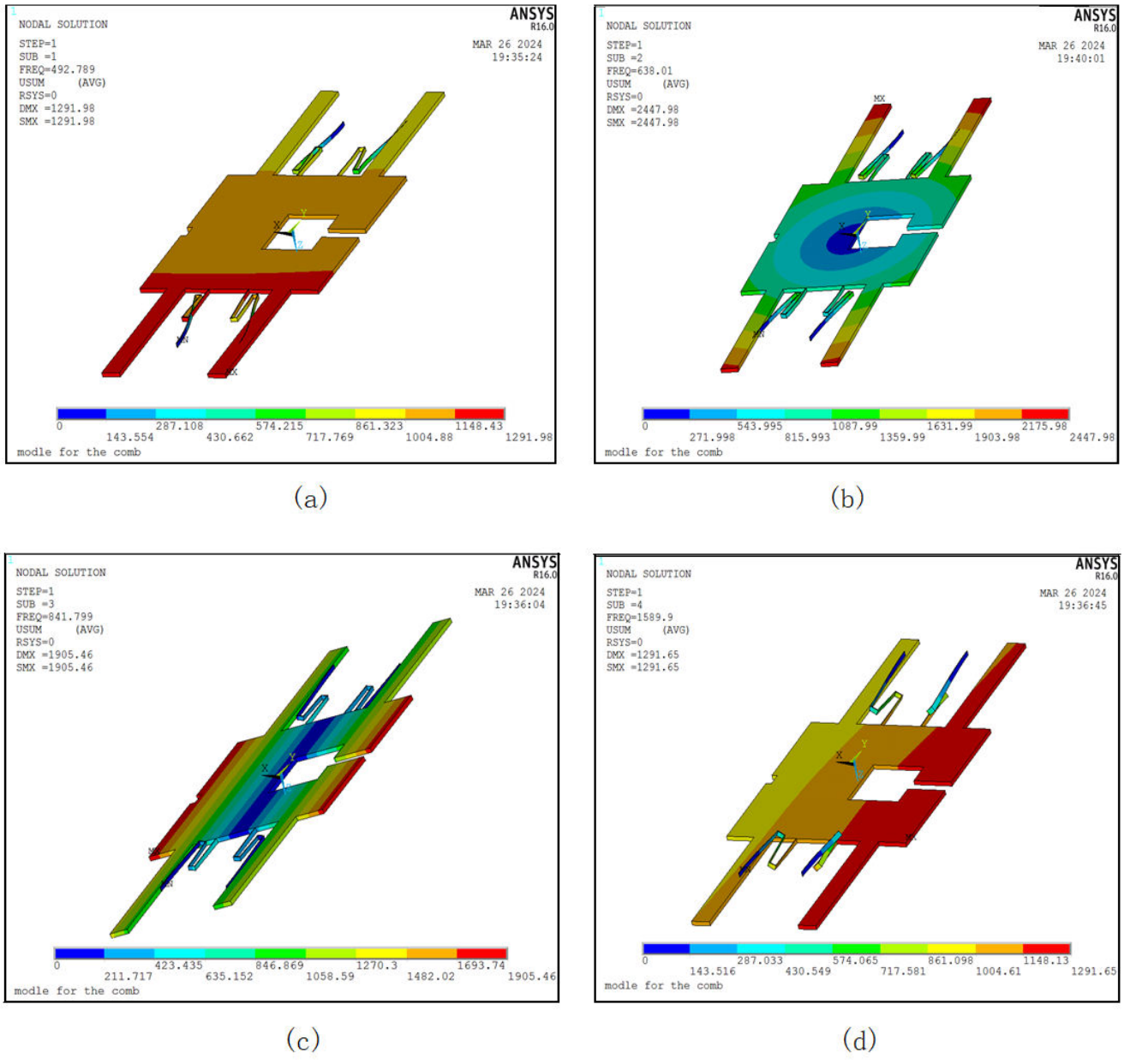

Figure 7: Results of the (a) First frequency mode, (b) Second frequency mode (c) Third frequency mode (d) Fourth frequency mode

| e-ISSN: 2278 – 8875, p-ISSN: 2320 – 3765| www.ijareeie.com | Impact Factor: 8.317|| A Monthly Peer Reviewed & Referred Journal |

||Volume 13, Issue 4, April 2024||

|DOI:10.15662/IJAREEIE.2024.1304001 |

3.4. Dynamic modulation of the reconfigurable antenna

The microwave performance of the proposed antenna is simulated successfully using HFSS software. With a variation of the S parameter, the corresponding returns loss results are displayed in Figure 8. When the spacing between the tuning stub and the quadrilateral ring slot is increased from 40 to 60µm, the return losses at S_{11} < -10 dB fall below -12dB, and there is a drop in the bandwidth from 204 to 155MHz (0.334 to 0.256%). Furthermore, when the spacing is increased from 60 to 65, the return loss records fall below 14dB, and there is a slight rise in the bandwidth from 155 to 170 MHz (0.256 to 0.28%). This demonstrates a broad bandwidth with a continuously changing frequency range from 59.72 to 60.8 GHz. To obtain good RF performance of the antenna, the impedance matching of the antenna is increased.

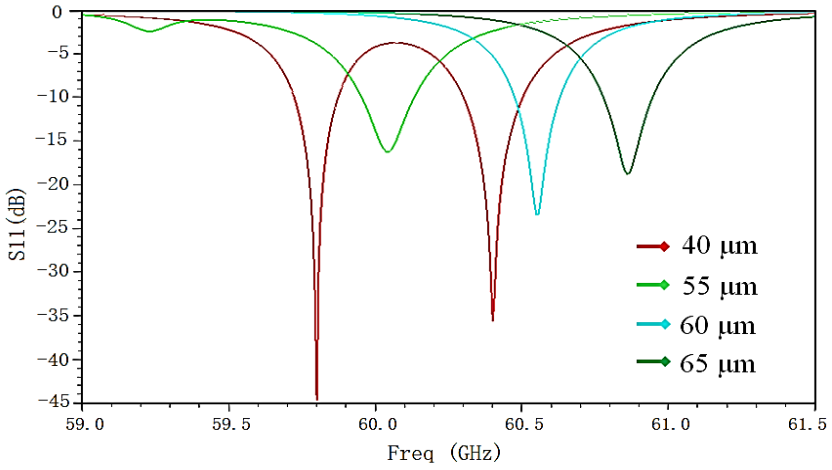

Figure 8: Return loss for various S parameters

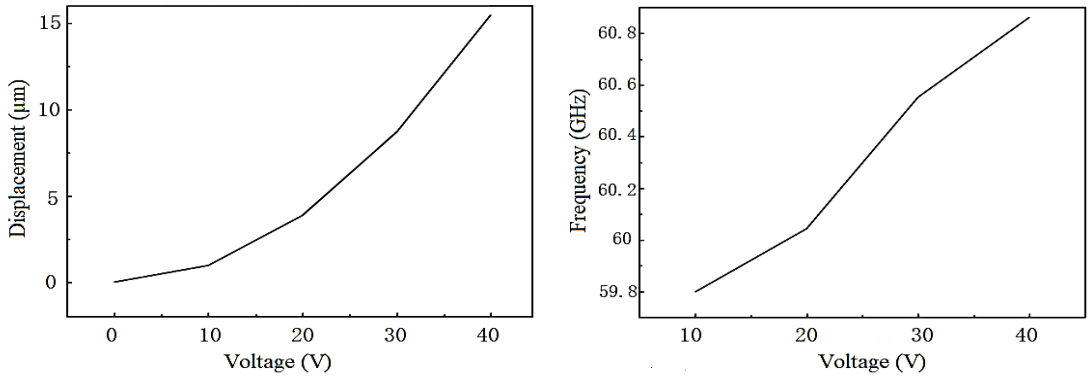

(a) Displacement vs drive Voltage (b) Antenna Frequency vs drive Voltage

Figure 9: Dynamic modulation results

IV. CONCLUSION

The design of a proposed miniaturized reconfigurable CPW antenna with a widened tuning frequency region based on MEMS technology has an overall size of 2 mm x 2 mm, which makes it good for miniaturization. The antenna is printed on a silicon substrate material. The proposed antenna shows a good performance in terms of return losses. To achieve a good impedance match for this proposed antenna, the gap between the stub and the quadrilateral ring slot is altered mechanically at certain displacements to realize the desired radiation frequencies which is achieved by a bias voltage of 10 to 40V. At a bias voltage of 40V, the MEMS actuator performs a maximum displacement of 15.5 µm driven by a stress of 40mpa, and the frequency of the antenna shifts from 59.79GHz to 60.4GHz. Based on the mm-wave band range, this proposed antenna is suitable for high-speed wireless communications and radar systems.

| e-ISSN: 2278 – 8875, p-ISSN: 2320 – 3765| www.ijareeie.com | Impact Factor: 8.317|| A Monthly Peer Reviewed & Referred Journal |

||Volume 13, Issue 4, April 2024||

|DOI:10.15662/IJAREEIE.2024.1304001 |

REFERENCES

[1] Tarek Djerafi and K. We," Super-compact substrate integrated waveguide cruciform directional coupler", IEEE Microwave and wireless components letters, Vol.17, No 11.
[2] Chao Wang, Wenquan Che, Chao Li, and Dongtian Liu, "Multiway microwave planar power divider/combiner based on substrate integrated rectangular waveguide directional couplers", Microwave and Optical Technology, .50, N6, June 2008.
[3] Y. J. Cheng, K. Wu, and W. Hong, "Substrate integrated waveguide (SIW) broadband compensating phase shifter," IEEE MTT-S Int. Microwave. Symp. Dig.
[4] Asanee Suntives, and Ramesh Abhari, "Transition structures for 3-D integration of substrate integrated Waveguide interconnects," IEEE Microwave and wireless components letters, Vol. 17, October 2007.
[5] C. G. Christodoulou, Design of reconfigurable antennas using graph models. San Rafael, CA, USA: Morgan and Claypool, 2013.
[6] C. G. Christodoulou, Y. Tawk, S. A. Lane, and S. R. Erwin, ''Reconfigurable antennas for wireless and space applications,'' Proc. IEEE, vol. 100, no. 7, Jul. 2012.
[7] L. Jin, R. M. Lee, and I. D. Robertson, "Design and performance of log-periodic substrate integrated waveguide slot antennas," in 2012 IEEE/MTT-S International Microwave symposium digest, June 2012.
[8] Munk, B.A. Frequency selective surfaces: Theory and design; Wiley Online Library: Hoboken, NJ, USA, 2000; Volume 29.
[9] Vardaxoglou, J.C. Frequency selective surfaces: analysis and design; Research Studies Press: Boston, MA, USA, 1997
[10] J. Yeo, Y. Lee, and R. Mittra, Wideband slot antennas for wireless communications, IEEE Proc Microwaves Antenna Propag. 151 (2004), 351–355.
[11] R. Chair, A. Kishk, and K. Lee, Ultra-wideband coplanar waveguide fed rectangular slot antenna, IEEE Antenna wireless propag. letter 3 (2004), 227–229.
[12] Khurshid, A.; Dong, J.; Shi, R. A Metamaterial-based compact planar monopole antenna for Wi-Fi and UWB applications. Sensors 2019, 19, 13.
[13] Kim, J.; Sung, Y. Dual-band microstrip patch antenna with switchable orthogonal linear polarization.J. Electromagnet. Eng. Sci. 2018, 18, 215. 20.
[14] J. Yeo, Y. Lee, and R. Mittra, Wideband slot antennas for wireless communications, IEE Proc Microwaves Antenna prop. 151 (2004), 351–355.
[15] S.-W. Qu, C. Ruan, and B.-Z. Wang, Bandwidth enhancement of wide-slot antenna fed by cpw and microstrip line, IEEE Antenna wireless prop. letter 5 (2006), 15–17.
[16] C. G. Christodoulou, Design of reconfigurable antennas using graph models. San Rafael, CA, USA: Morgan and Claypool, 2013.
[17] C. G. Christodoulou, Y. Tawk, S. A. Lane, and S. R. Erwin, ''Reconfigurable antennas for wireless and space applications,'' Proc. IEEE, vol. 100, no. 7.
[18] L. Giauffret, J. M. Laheurte, and A. Papiernik, "Study of various shapes of the coupling slot in cpw-fed microstrip antennas," IEEE Trans. Antennas propag, vol. 45, no. 4.
[19] X. -S. Yang, B. -Z. Wang, W. Wu and S. Xiao, "Yagi Patch Antenna with dual-band and pattern reconfigurable Characteristics." IEEE Antennas and wireless propagation letters, vol. 6.
[20] Aboufoul, T.; Chen, X.; Parini, C.; Alomainy, A. (2014). "Multiple-parameter reconfiguration in a single planar ultra-wideband antenna for advanced wireless communication systems". IET Microwaves, Antennas & Prop. 8 (11): 849–857.
[21] H. Chen, Z. Shi, L. Wu and D. Guo, "Frequency reconfigurable antenna with micromechanical patch," 2007 International workshop on anti-counterfeiting, security, and Identification (ASID), Xizmen, China, 2007.
[22] Liu C. Micromachinery: foundations of MEMS [M]. Huang Q A, Transl. 2nd ed. Beijing: China Machine Press, 2013: 381.

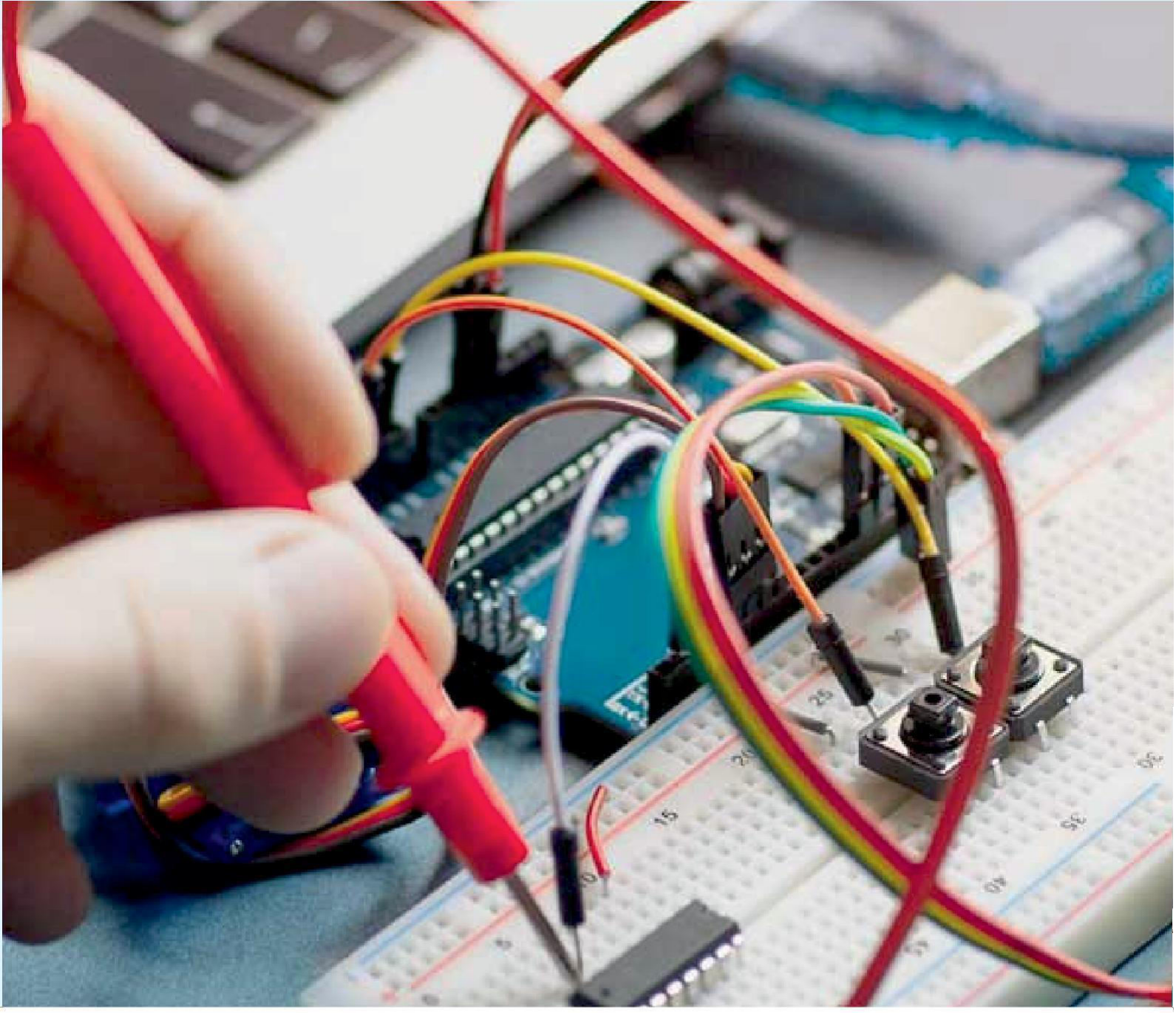

INNO SPACE
SJIF Scientific Journal Impact Factor

doi cross ref

ISSN INTERNATIONAL STANDARD SERIAL NUMBER INDIA

निस्केयर NISCAIR

International Journal of Advanced Research

in Electrical, Electronics and Instrumentation Engineering

9940 572 462 6381 907 438 ijareeie@gmail.com

Scan to save the contact details